JCTC Journal of Chemical Theory and Computation

Stability of K-Montmorillonite Hydrates: Hybrid MC Simulations

G. Odriozola* and J. F. Aguilar

Programa de Ingeniería Molecular, Instituto Mexicano del Petróleo, Lázaro Cárdenas 152, 07730 México, D. F., México

Received March 9, 2005

Abstract: $NP_{zz}T$ and $\mu P_{zz}T$ simulations of K-montmorillonite hydrates were performed employing hybrid Monte Carlo simulations. Two condition sets were studied: $P = 1$ atm and $T = 300$ K (ground level conditions) and $P = 600$ atm and $T = 394$ K; this last condition mimics a burial depth close to 4 km. For these conditions, swelling curves as a function of the reservoir water vapor pressure were built. We found the single layer K-montmorillonite hydrate stable for high vapor pressures for both burial and ground level conditions. A simple explanation for this high stability is given.

I. Introduction

Clays are layer type aluminosilicate minerals, existent everywhere in nature and industry, hence the importance of a detailed understanding of their physics and chemistry. They are used as building materials, ceramics, and catalysts; they are employed in cosmetics, as rheological modifiers for paints, and in technological processes such as oil well drilling. In this last application, the control of their stability is a key for drilling success. During it, the use of water based muds induce destabilization of shale and clay formations that would disintegrate, or heave, upon contact with water.

One way to maintain stability of shales during the drilling process is by addition of potassium salts to drilling muds. This helps to avoid fluid loss and water infiltration. These kind of muds, that contain potassium ions dissolved in the water phase, are widely used for drilling water-sensitive shales, specially hard, brittle shales. Potassium cations in these systems replace ions such as sodium found in most shales to produce less hydrated clays with significantly reduced swelling potential. These ions also help to hold the cuttings together, minimizing their dispersion into finer particles. From all of the previous facts, a good understanding of the role of potassium in the swelling clays such as montmorillonite is mandatory, in particular at basin conditions of hard experimental implementation.

Besides the experimental studies, computer simulations are essential components of research on clay−water−cation systems.[1−13] These simulations give microscopic insights that are difficult to access experimentally. There are, however, not many computational studies on the swelling of montmorillonite hydrates for potassium interlayer cations.[14−20] In addition, excluding Hensen et al.[7,17] and Tambach et al.[20] works, these papers report solely $NP_{zz}T$ and NVT simulations, where the number of water molecules per interlaminar space is someway arbitrarily fixed, and hence, they do not show the whole picture of swelling. A good example of this is that hysteresis is naturally predicted by sampling in an open ensemble,[4,7,21] without the need of measuring properties such as water chemical potential,[9] immersion energies,[13] or swelling free energies.[12,22] Finally, this paper focuses on the stability of the different hydrates in contact with several reservoirs, which differ in temperature, pressure, and water activity.

The importance of potassium as swelling inhibitor of clays and the above-mentioned reasons motivated us to study the microscopic mechanisms underlying the behavior of K-montmorillonite hydrates at equilibrium with different reservoirs. We performed simulations of these systems in the $NP_{zz}T$ and $\mu P_{zz}T$ ensembles, considering explicitly two clay layers in the simulation box to avoid finite size effects. The simulations were carried out for two condition sets. One at ground level, with $P = 1$ atm and $T = 298$ K, and the other one with $P = 600$ atm and $T = 394$ K, which corresponds to an average burial depth close to 4 km.

* Corresponding author phone: +5255 91758176; e-mail: godriozo@imp.mx.

10.1021/ct050062l CCC: $30.25
Published on Web 09/20/2005

The paper is organized as follows. In section II, we briefly describe the models and the methodology employed for performing the simulations. The results are shown in section III. Finally, section IV discusses the main results and extracts some conclusions.

II. Methodology

A. The Model. A 4 × 2 layer of Wyoming type montmorillonite clay was built up by replication of the unit cell given by Skipper et al.[23] This layer has $L_x = 21.12$ Å, $L_y = 18.28$ Å, and $L_z = 6.56$ Å dimensions. The Wyoming type montmorillonite was obtained by isomorphous substitutions of trivalent Al atoms of the octahedral sites by divalent Mg atoms and tetravalent Si by trivalent Al atoms. The unit cell formula of this clay is given by $K_{0.75}nH_2O(Si_{7.75}Al_{0.25})(Al_{3.5}Mg_{0.5})O_{20}(OH)_4$. Size effects were avoided by considering two layers in the simulation box.[4] Periodic boundary conditions were imposed on the three space directions. The initial configuration consists of water molecules randomly placed in the interlaminar spaces and six potassium ions distributed in the interlayer midplanes. These counterions balance the negative charge of the clay framework keeping the system electroneutral.

The rigid TIP4P model was used for water molecules,[20,24] and the water clay interactions were taken from Boek et al.[1] Here, site-to-site intermolecular interactions are given by electrostatic and Lennard-Jones contributions

$$U_{ij} = \sum_{a,b}\left[\frac{q_a q_b}{r_{ab}} + 4\epsilon_{ab}\left[\left(\frac{\sigma_{ab}}{r_{ab}}\right)^{12} - \left(\frac{\sigma_{ab}}{r_{ab}}\right)^{6}\right]\right] \quad (1)$$

where subindexes i and j are for molecules, and a and b run over all sites of each molecule. q_a and q_b are the corresponding site charges, ϵ_{ab} and σ_{ab} are site-to-site specific Lennard-Jones parameters, and r_{ab} is the intersite distance. The Lennard-Jones parameters for single sites are shown in Table 1. Here, those parameters for Si were taken from Marry et al.,[25] and parameters for Al and Mg were assumed to be equal to those of Si. The site-to-site Lennard-Jones parameters are given by the Lorentz−Berthelot rules

$$\sigma_{ab} = \frac{\sigma_a + \sigma_b}{2} \quad (2)$$

$$\epsilon_{ab} = \sqrt{\epsilon_a \epsilon_b} \quad (3)$$

On the other hand, the K−H_2O interactions and those between the oxygens of the clay and potassium ions are based on the ones proposed by Bounds.[26] Bounds potential is chosen since, while simple, it produces K-TIP4P radial distribution functions in agreement with available experimental data and close to those obtained by hybrid quantum mechanics/molecular mechanics (QM/MM) simulations, which naturally account for the many body contributions to the potential.[27] That is, the K−O radial distribution function peaks at 2.86 Å leading to a first shell oxygen coordination number of 7.6, while high accuracy QM/MM simulations performed at density functional theory level (LANL2DZ basis set) give 2.81 Å of K−O distance and 8.3 of coordination number. Experimental results give K−O distances between 2.7 and 3.1 Å and coordination numbers in the wide range of 4−8.[28,29] He fitted the following pair potential for the K−H_2O dispersion−repulsion contribution obtained from ab initio calculations

Table 1: Lennard-Jones Parameters for H_2O−Clay−K Interactions[a]

sites	ϵ (kcal/mol)	σ (Å)
O	0.155	3.1536
H	0.000	0.0000
K	3.630	2.4500
Si	3.150	1.8400
Al	3.150	1.8400
Mg	3.150	1.8400

[a] Exceptions are the K−O and K−H interactions.

$$U_{K-H_2O} = A_{KO}\exp(-b_{KO}r_{KO}) - C_{KO}/r_{KO}^4 - D_{KO}/r_{KO}^6 + A_{KH}\exp(-b_{KH}r_{KH_1}) + A_{KH}\exp(-b_{KH}r_{KH_2}) \quad (4)$$

yielding $A_{KO} = 53884.0$ kcal/mol, $b_{KO} = 3.3390$ Å^{-1}, $C_{KO} = 438.0$ kcal Å^4/mol, $D_{KO} = -638.0$ kcal Å^6/mol, $A_{KH} = 5747.0$ kcal/mol, and $b_{KH} = 3.4128$ Å^{-1}. This intersite potential, although somewhat more complicated than the Lennard-Jones type, produces a much better match to the ab initio data.[26] This is clearly seen if one tries to fit eq 4 with a Lennard-Jones type potential. In fact, parameters shown in Table 1 for potassium were obtained by this way, yielding a poor match although reproducing the depth and position of the pair-potential minimum. We observed that the discrepancies are very pronounced at short distances, where the Lennard-Jones potential shows a much harder behavior. This explains why Boek et al. found a very large dehydrated interlaminar space when they employed a Lennard-Jones type pair potential for K−O.[14] Naturally, they overcome this difficulty by employing the pair potential proposed by Bounds.[26]

Nevertheless, since it is crucial for the hybrid Monte Carlo simulations to keep the energy fluctuations as low as possible in order to enlarge the acceptation rate,[30] it is convenient to avoid employing relatively long-range pair potential contributions such as $\sim r^{-4}$, if no Ewald treatment is applied on them. Hence, we refitted to eq 4 the following expression

$$U_{K-H_2O} = A_{KO}\exp(-b_{KO}r_{KO}) - C_{KO}/r_{KO}^6 + A_{KH}\exp(-b_{KH}r_{KH_1}) + A_{KH}\exp(-b_{KH}r_{KH_2}) \quad (5)$$

by employing a Levenberg−Marquardt algorithm and considering several K−H_2O configurations. The procedure yields $A_{KO} = 120750.2$ kcal/mol, $b_{KO} = 3.4110$ Å^{-1}, $C_{KO} = 5153.8$ kcal Å^6/mol, $A_{KH} = 2109.4$ kcal/mol, and $b_{KH} = 2.8515$ Å^{-1}. We observed that avoiding the $\sim r^{-4}$ term the acceptance rate enlarges more than three times for a small (inner) time step of 0.8 fs. In general, both functions yield similar values of the K−H_2O potential energy. Minima are located practically at the same distance although the depth of the fitted function is 5% larger. For larger distances this difference decreases. To check the obtained interaction potential, a *NPT* simulation containing 216 water molecules, a potassium cation, and a chloride anion was performed at $P = 1$ atm and $T = 293$ K.

The corresponding K−O and K−H radial distribution functions, $g(r)$, and coordination numbers, $n(r)$, were studied. These functions were observed to be very similar to those reported by Bounds.[26] That is, the K−O and K−H main peaks are located at 2.83 and 3.29 Å, respectively, which compare well with their corresponding values of 2.86 and 3.32 Å.[26] The coordination number for the $g(r)$ minimum was found at 7.7 Å, in agreement with his value of 7.6 Å.[26] Moreover, all these values are even closer to the results obtained by QM/MM simulations.[27] Hence, expression 5 seems to be suitable for our purposes.

Finally, we should mention that electrostatic contributions, $\sim r^{-1}$, were treated through the implementation of the Ewald summation formalism. Here the convergence factor was fixed to $5.6/L_{min}$, where L_{min} is the minimum simulation box side. There were set five reciprocal lattice vectors for the directions along the shortest sides and six vectors for the direction along the largest side.[31] The dispersion−repulsion contributions were corrected using the standard methods for homogeneous fluids,[32] and a spherical cutoff of $L_{min}/2$ was imposed.

B. Simulations. Simulations were performed employing the hybrid Monte Carlo (HMC) method.[21,30] This technique allows making global moves while keeping a high average acceptance probability. Global moves are done as follows from molecular dynamics (MD), i.e., by assigning velocities and by using a particular scheme for integrating the Newton's equations of motion. Velocities are assigned randomly from a Gaussian distribution in correspondence with the imposed temperature and in such a way that total momentum equals zero for both interlaminar spaces. To fulfill detail balance condition, the discretization scheme must be time reversible and area preserving.[30] In particular, we employed the multiple time scale algorithm given by Tuckerman and Berne.[33] This algorithm has the property of splitting the forces into short and long range. The Lennard-Jones contribution plus the real part of the electrostatic forces are set as short range, and the reciprocal space contribution of the electrostatic forces is set as long range. To decrease time correlations a new configuration is generated each 10 integration steps. The probability to accept this new configuration is given by

$$P = \min\{1, \exp(-\beta\Delta H)\} \quad (6)$$

where ΔH is the difference between the new and previous configuration Hamiltonians, and β is the inverse of the thermal energy. The long time step is set to 8 times the short time step, and the short time step is chosen to obtain an average acceptance probability of 0.7.[30] This way, we obtained short time steps close to 1.0 and 0.5 fs for systems containing 10 and 100 water molecules per interlaminar space, respectively. As can be seen, the time step shortens with increasing the system size, since energy fluctuations enlarge. This is why HMC is not very efficient for systems counting on a large number of movable sites. This is not our case, since few ions and water molecules are the only contributors to energy fluctuations. This makes HMC a reasonable choice. In fact, the time steps we are obtaining are similar to those usually employed for typical MD calculations.[5,11,20,25]

For sampling in the $NP_{zz}T$ ensemble, after a trial change of particles' positions, a box change is attempted in such a way that the stress normal to the surface of the clays, P_{zz}, is kept constant. For this purpose, box fluctuations are allowed only in the z-direction, and the probability for accepting the new box configuration is given by

$$P = \min\{1, \exp[-\beta(\Delta\mathcal{U} + P_{zz}\Delta V - N\beta^{-1}\ln(V_n/V_o))]\} \quad (7)$$

Here, $\Delta\mathcal{U}$ is the change in the potential energy, ΔV is the volume change, N is the total number of molecules, and V_n and V_o are the new and old box volumes, respectively.[4]

For sampling in an open ensemble, the possibility of insertions and deletions of water molecules has to be considered. Water insertions and deletions were performed by Rosenbluth sampling.[17,21] The $\mu P_{zz}T$ ensemble[21] was used to obtain the equilibrium states when the system is in contact with a reservoir at certain temperature, pressure, and water chemical potential. For this purpose, the algorithm must sample the probability density of finding the system in a particular configuration, i.e.,

$$\mathcal{N}_{\mu PzzT} \propto \frac{V^N \exp\{-\beta[\mathcal{U} - \mu N + P_{zz}V]\}}{\Lambda^{3N}N!} \quad (8)$$

Hence, particle movements, insertions, deletions, and box changes must be done as in a typical NVT, μVT, and $NP_{zz}T$ sampling.[34] In particular, after trying a change of particles' positions, we performed tries of inserting−deleting water molecules. This is done by randomly calling both possible trials in such a way that calls are equally probable. Since accepting insertions or deletions are rare, we repeat this step 10 times or until any insertion or deletion is accepted. In case of refusing the 10 insertion−deletion trials, we performed a box trial move.[35] In this way, the system rapidly evolves to an equilibrium state. For some conditions, however, two free energy local minima appear, which are accessed by handling initial conditions.

III. Results

Results are presented in two subsections. These are *Sampling in the $NP_{zz}T$ Ensemble* and *Sampling in the $\mu P_{zz}T$ Ensemble*. Each part presents the results for ground level conditions, i.e, $T = 298$ K and $P = 1$ atm, and for 4 km of burial depth, i.e, $T = 394$ K and $P = 600$ atm, assuming average gradients of 30 K/km and 150 atm/km.

A. Sampling in the $NP_{zz}T$ Ensemble. Let us first focus on the swelling behavior of the K-montmorillonite hydrates under ground level conditions. This is shown as a plot of the interlaminar distance as a function of the number of water molecules obtained by $NP_{zz}T$ simulations. This curve starts from a dehydrated state having an interlaminar distance of 10.4 Å, which is somewhat larger than the experimental value of 10.1 Å.[36] For a small number of water molecules, the system reaches interlaminar distances above 11 Å, which slightly increases with increasing the number of water molecules producing a plateau. This plateau shows interlaminar distances in the range 11.3−12.3 Å, which are clearly lower than those produced by Na-montmorillonite.[4,9]

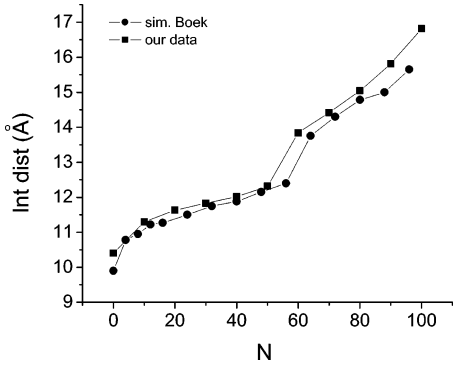

Figure 1. Interlaminar distance as a function of the number of water molecules per interlaminar space.

This might be seen as something unexpected, since potassium ions are much larger than sodium ions. As we comment ahead, this is due to the different interlayer structures that sodium and potassium ions generate. For 60 water molecules per interlaminar space, there is a jump from a single water layer to a double water layer, which yields an interlaminar distance of 13.9 Å. For larger amounts of water the system increases almost linearly, producing a very small step when jumping from a double to a triple water layer structure.

Our findings are similar to those reported by Boek et al.[14] We included them in Figure 1 to make the comparison easy. It is seen that trends are practically equal. This indicates that differences in models and methods are not very important. Nevertheless, they always obtain slightly smaller interlaminar distances for a given number of water molecules. This difference is always lower than 2%, except for the dehydrated state and the points close to 100 water molecules, where differences close to 5% are observed. Since in our case the jump from a single to a double layer is obtained for a lower amount of interlaminar water, the points that correspond to 55−60 water molecules also show a larger difference. Anyway, differences seem reasonable taking into account the differences in pair potential definitions, box sizes, and methodologies.

The structure of the interlaminar space for the system containing 40 water molecules per interlaminar space is shown in Figure 2. A high and narrow oxygen peak at the interlaminar midplane, three hydrogen peaks, one coinciding with the oxygen peak and the other two symmetrically situated at both sides, and a single potassium ion peak, also at the interlaminar midplane, are observed. Most of these results agree with others previously reported.[14,16,17] It should be noted that this structure contrasts with that one of the Na-montmorillonite single layer hydrate. In this case, sodium ions are distributed at the sides of the oxygen peaks, closer to the clay sheets, some of them being strongly attached to the clay surface and so forming inner-sphere surface complexes.[15] This makes water molecules to cluster in two layers joined at the interlaminar midplane, producing an oxygen double peak.[21,37] Naturally, this effect widens the interlaminar space, despite the smaller size of sodium ion.

The radial distribution functions and coordination numbers for K−O sites were also studied. Main $g(r)$ peaks are situated at 2.77, 2.90, and 2.83 Å for water, clay, and total oxygen

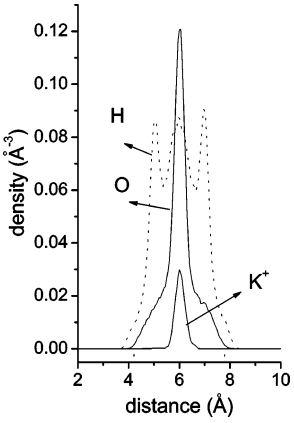

Figure 2. Oxygen, hydrogen, and potassium density profiles of the interlaminar space. The water amount was fixed to 40 molecules per interlaminar space.

sites, respectively. Although they are close to the one observed for bulk potassium water solution, a contraction is seen for the K−O water distance as a consequence of confinement. On the other hand, the relatively large K−O clay distance is due to the distribution of the potassium ions around the midplane of the interlayer space. The coordination numbers for the first shell of oxygen atoms are 5.1, 5.0, and 10.1 for water, clay, and total oxygen sites, respectively. The clay and total coordination numbers are somewhat inflated due to the smaller separation of the O−O sites of the clay. This explains why the total coordination number is larger than the one found for bulk. It should be noted the large contribution of the clay to the total coordination number. This suggests that potassium ions are interacting with both clay sheets at the same time. In addition, the large K−O clay distance may be indicating that potassium ions are directly contributing to attract both layers toward the midplane and hence holding the sheets close to one another.

All the already pointed features are illustrated in Figure 3. For instance, it is observed that potassium ions are practically centered on the interlayer midplane with an approximate average of 5 water molecules surrounding each ion. It is also possible to see how ions tend to separate from each other, and that one of them is always close to a tetrahedral aluminum (these sites are not highlighted in the figure). Moreover, it is shown that there are no water molecules interposed between the potassium ions and the clay sheets. Hence, potassium ions are behaving as inner-sphere complexes but simultaneously with both clay layers. To see this even clearer, Figure 4 was built by rotating and zooming in Figure 3. Here, a potassium ion and its inner water shell are shown. As can be seen, only 5 water molecules surround the ion that coordinates with two oxygen atoms from each clay. For this particular case, are also seen average K−O distances of 2.81 and 3.04 Å for water and clay, respectively.

As mentioned before, for 60 water molecules a double layer hydrate is formed. This double layer hydrate becomes fully developed for 80 water molecules, where an interlayer distance close to 15.0 Å is observed. For this system, the oxygen, hydrogen, and potassium profiles are shown in Figure 5. Here, the two oxygen peaks are a signature of the

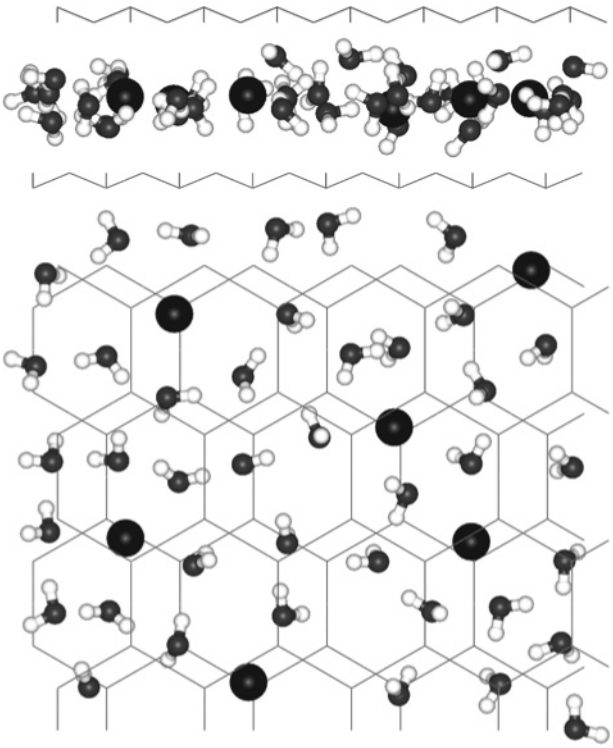

Figure 3. Snapshot of an equilibrated system having 40 water molecules. H sites are white, O are gray, and K are black. The wireframe represents the clay structure. The topmost image is a side view, and the lower image is the corresponding top view.

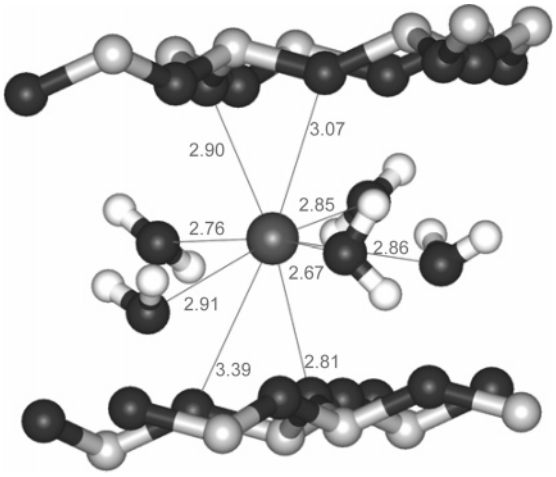

Figure 4. Zoom in of a potassium ion and its coordination shell taken from Figure 3. Only water molecules having K−O distances smaller than 3.7 Å are shown. Distances in the figure are given in Å.

double water layer structure. For each oxygen peak a potassium peak and two hydrogen peaks are found. The potassium peak is found almost coinciding with the oxygen peak but slightly displaced at the side closer to the clay sheet. This suggests the formation of inner-sphere complexes. On the other hand, a small hydrogen peak is found at the side closer to the clay sheet and a larger one closer to the interlaminar midplane. Hence, the third hydrogen peak found for the one layer case is missing here.

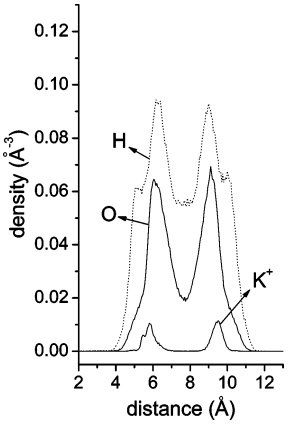

Figure 5. Oxygen, hydrogen, and potassium density profiles of the interlaminar space. The water amount was fixed to 80 molecules per interlaminar space.

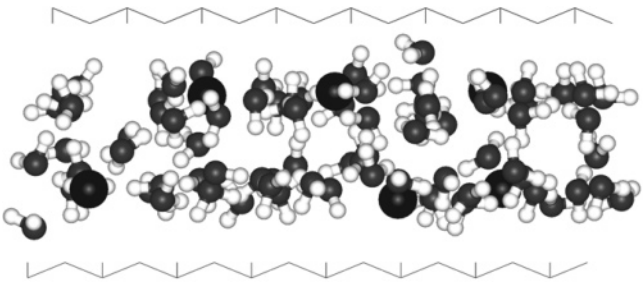

Figure 6. Snapshot of an equilibrated system having 80 water molecules per interlaminar space. H sites are white, O are gray, and K are black. The wireframe represents the clay structure.

For this configuration, main $g(r)$ peaks are located at 2.83, 2.75, and 2.79 Å for water, clay, and total oxygen sites, respectively. Hence, the K−O distance for water is not contracted anymore but equal to the bulk water K−O distance. On the contrary, the K−O distance for the clay decreased 0.17 Å. Moreover, this distance is found to be almost constant for systems having more than 60 water molecules, strongly suggesting that this is the natural average K−O distance for a potassium ion attached to the siloxane surface. Hence, the distance found for the single layer hydrate would be elongated as a result of the pressure the water molecules produce on the clay surfaces. The corresponding coordination numbers are 6.8, 2.8, and 9.6 for water, clay, and total oxygen sites, respectively. As can be seen, the coordination number for the clay is much lower than the value found for the single layer hydrate. This means that potassium ions are coordinated to only one clay layer for the double layer hydrate. Finally, and as expected, K−O water coordination numbers increase with the number of water molecules, whereas K−O clay and K−O total coordination numbers decrease. A snapshot of this two layer hydrate is shown in Figure 6. We should mention that the structure of the inner-sphere complexes we found in this case are very similar to those already reported by Sposito et al.[19] (not shown here).

For burial conditions the interlaminar distance increases for a given number of water molecules per interlaminar space. This is shown in Figure 7, where it shows the

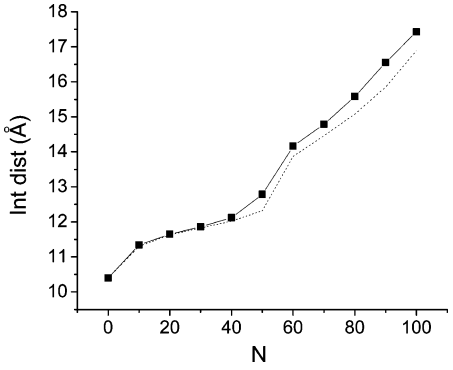

Figure 7. Interlaminar distance as a function of the number of water molecules per interlaminar space for burial conditions. For comparison, the dotted line corresponds to ground conditions (from Figure 1).

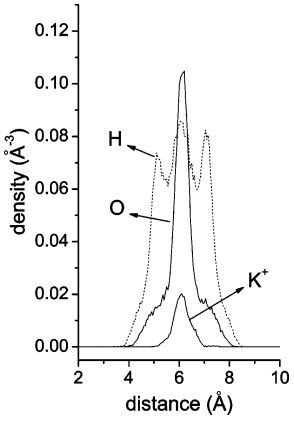

Figure 8. Oxygen, hydrogen, and potassium density profiles of the interlaminar space. The water amount was fixed to 40 molecules per interlaminar space for burial conditions.

interlaminar distance as a function of the number of water molecules for burial and for ground level conditions. This increment is more pronounced for large amounts of water. This is an expected behavior since water molecules occupy larger effective volumes at burial conditions.[9] Consequently, profiles turn less sharp, i.e, peaks broad and shorten, as it is shown in Figure 8. This was seen experimentally by Skipper et al., although for a Na-montmorillonite system.[38] On the other hand, trends for both the ground and burial data are very similar, i.e, jumps are found at equal numbers of water molecules. This last finding differs from the one found for Na-montmorillonite, where the single layer to double layer jump occurs for 60 or 50 water molecules, depending on the burial depth.[9]

B. Sampling in the $\mu P_{zz}T$ Ensemble. Sampling in this ensemble allows the system to reach equilibrium with a reservoir whose temperature, pressure, and, in our case, water chemical potential are fixed. We employed the expression $\beta\mu = \beta\mu_0 + \ln(p/p_0)$, where p_0 is the vapor pressure at equilibrium with liquid water whose chemical potential is μ_0, and p is the vapor pressure. For the TIP4P water model with $T = 298$ K and $P = 1$ atm, we employed $\beta\mu_0 = -17.4$. This value was obtained by *NPT* simulations of bulk TIP4P water[21] and using the Rosenbluth sampling method explained elsewhere.[17,34] It is in good agreement with the value reported by Chávez-Páez et al.,[4] and it is 2.5% larger than the one

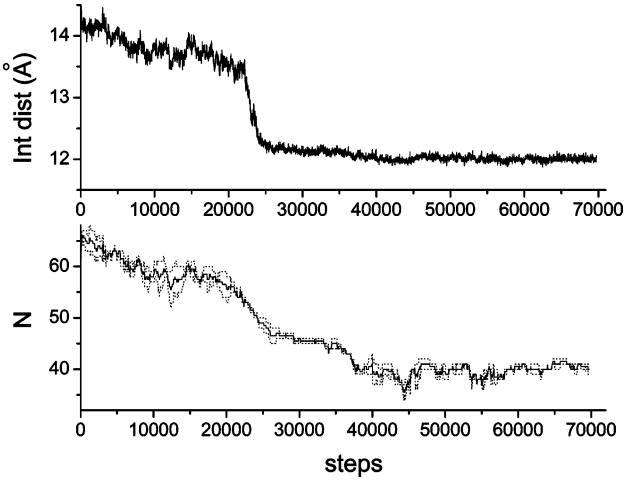

Figure 9. Step evolution of the interlaminar distance and number of water molecules obtained by $\mu P_{zz}T$ sampling. In the lower plot, dashed lines correspond to each interlaminar space, whereas the solid line is the average. Initial conditions were 16 Å and 60 water molecules per interlaminar space. Established conditions were $T = 298$ K, $P = 1$ atm, and $p/p_0 = 0.4$.

reported by Tambach et al.[20] For $T = 394$ K and $P = 600$ atm, $\beta\mu_0 = -13.4$ was obtained.[21]

The evolution of the interlaminar distance and number of water molecules for ground level conditions and for $p/p_0 = 0.4$ is shown in Figure 9. Here, the initial conditions were 16 Å for the interlaminar distance and 60 water molecules per interlaminar space. It is observed that the system reaches approximately 65 water molecules and 14.3 Å of interlaminar distance at the initial simulation steps. This happens so fast since the system is initially very far from equilibrium. Immediately after, the system starts slowly losing water molecules and decreasing its interlaminar distance on its way toward equilibrium. It is observed that, once the system reaches 13.5 Å of interlaminar space, it quickly falls down to 12.2 Å, losing many water molecules during the process. This is a signature of the transition from a double layer hydrate to a single layer hydrate. The amount of water that signals the transition goes from 55 to 45 molecules. This agrees with the $NP_{zz}T$ results, where a single to a double layer transition is observed in the range of 40−60 water molecules and 12.2−14.3 Å. After the transition, it is observed that the system takes several steps to finally reach equilibrium at approximately 40 000 steps. In this case, sampling was performed in the step range of 40 000−70 000. For this particular run 12.0 Å of interlaminar space and 39.3 water molecules were obtained.

Many runs were performed in order to build up Figure 10. For ground level conditions, this figure shows the interlaminar distance and number of water molecules at equilibrium with reservoirs having different water vapor pressures. For zero vapor pressure, no matter what the established initial conditions, the system is forced to eliminate all of its water content, and so, the dehydrated state is yielded. This has 10.40 Å of interlaminar space, as was found in the preceding section. For increasing the vapor pressure, the system starts to uptake water molecules from the reservoir

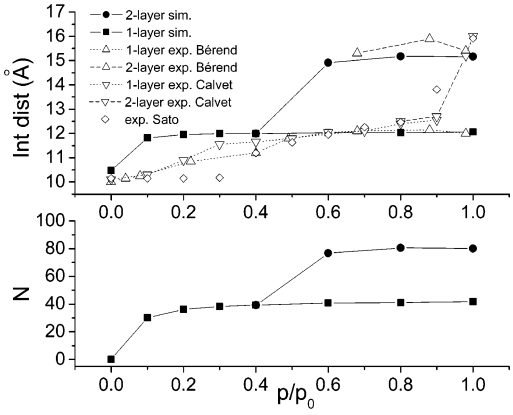

Figure 10. Interlaminar distance and number of water molecules per interlaminar space as a function of the vapor pressure for ground level conditions. Symbols □ and ○ correspond to initial conditions of 10 water molecules and 11.5 Å of interlaminar distance and 60 water molecules and 16.0 Å of interlaminar distance, respectively.

producing larger interlaminar distances. Nevertheless, the first water layer saturates for vapor pressures over $0.2p_0$, and so, a plateau is generated. Again, this single layer hydrate is produced for $p/p_0 \leq 0.4$ for all initial conditions.

For higher vapor pressures, however, at least two equilibrium states are yielded. That is, depending on the established initial conditions, the system may produce a double or a single layer hydrate. Hence, the topmost lines of both plots of Figure 10 correspond to an initial configuration of 60 water molecules and the others to an initial configuration of 10 water molecules. These two equilibrium states are stable up to water vapor saturation, producing an open hysteresis cycle. The single layer state yields interlaminar distances ranging in 11.82−12.06 Å and amounts of water in the range of 30.1−41.8 molecules. The double layer state produces interlaminar distances in the range 14.91−15.16 Å and numbers of water molecules ranging in 76.7−80.6. These data contrast with those obtained for Na-montmorillonite.[21] In this case, both initial conditions predict only a single layer hydrate for $p/p_0 \leq 0.2$. In addition, this single layer hydrate yields values of the interlaminar distance in the range of 12.34−12.73 Å, having 34.6−47.5 water molecules.[21] Therefore, it becomes evident the K-montmorillonite tendency to produce single layer hydrates even for relatively high vapor pressures and the small interlaminar distance and amounts of water it yields. On the other hand, the double layer plateaus for potassium and sodium do not behave very differently for high vapor pressures.

We should also compare our results with the experimental data obtained by Bérend et al.,[39] Calvet,[36] and Sato et al.[40] For this purpose, these data are also included in Figure 10. It should be pointed out that these data are direct measurements of interlaminar distances against the relative vapor pressure. Here, Bérend et al.'s data were obtained as the evolution of the interlaminar distance for a dehydration process, by starting from a double or a single layer hydrate. Similarly, Calvet presents his data by starting from a double or a single layer hydrate, but for a hydration process. Sato et al.'s data are also obtained by hydration.

The best agreement between our simulations and experiments is produced when comparing with the data of Bérend et al.[39] We highlight the double layer hydrate formation for the range of relative vapor pressures of 0.6−1.0; the single layer hydrate which keeps stable even for saturated vapor pressures; the very good agreement for the basal space for the single layer hydrate; and the relative good agreement for the double layer hydrate interlaminar distance, close to 15.5 Å. Calvet's data also are in general agreement with our simulations. He observed a very stable single layer hydrate, with interlaminar distances ranging in 11.8−12.5 Å. Nevertheless, he obtained a very unstable double layer hydrate. Only for relative vapor pressures of 0.9−1.0 this hydrate was observed. Its interlaminar distance is in the range of 15.2−16.0 Å. Sato et al.'s data also lead to similar interlaminar distances for the single and double layer hydrate. Finally, the single layer hydrate interlaminar distances also well agree with data reported by Brindley and Brown.[41] For 0.32, 0.52, and $0.79p_0$ of vapor pressure they reported 11.9, 11.9, and 12.1 Å, respectively.

On the other hand, the most important discrepancy with experiments is that they obtained interlaminar distances close to 10.0 Å for the dehydrated state, which seems to be stable up to a relative vapor pressure ranging in 0.1−0.3. We think that if we were capable of reproducing the correct dehydrated distance, i.e., 10.0 instead of 10.4 Å, this state would probably become stable for small vapor pressures, as they found.

Experimentalists agree that for relative vapor pressures ranging from 0.0 to 0.4, a mixture of the dehydrated state and the single layer hydrate coexists, i.e., there is interstratification. Similarly, they observed the coexistence of double and single layer hydrates, for high relative vapor pressures. In fact, Calvet refers to his own data as "apparent distances"; Bérend et al. conclude that all montmorillonites (they studied Li, Na, K, Rb, and Cs-montmorillonites) form interstratified hydrates; and Sato et al. observed several "nonintegral basal reflections", which are interpreted as "random or segregated-type interstratification of collapsed and expanded layers". An example is the 13.81 Å of interlaminar distance he obtained for the relative vapor pressure of 0.9. This point does not match either a single or a double hydrate interlaminar distance, as it is clearly seen in Figure 10. It is important to mention that the general belief is that interstratification occurs due to chemical heterogeneities of the clay layers. It was already proven by simulations that changes on the positions of the clay substitutions produce different interlaminar distances (although differences are not very pronounced). Hence, these heterogeneities surely lead to quasihomogeneous states and, probably, to interstratified ones. On the other hand, a perfect system like ours shows the double and the single layer hydrates to be stable for identical conditions. Hence, we do not see any reason for this not to occur in a real system. In other words, we think that this is another source of interstratification, which arises just as a consequence of the inherent thermodynamics of the perfect system. In fact, similar conclusions are deduced by Tambach et al.[22]

Table 2: *g*(*r*) Main K−O Peak Positions, *p*, and First Shell Coordination Numbers, *n*, for Systems under Different Water Vapor Pressures, p/p_0[a]

	single water layer				double water layer			
p/p_0	p_w	p_c	n_w	n_c	p_w	p_c	n_w	n_c
0.1	2.77	2.83	4.83	5.32				
0.2	2.77	2.85	4.96	5.11				
0.3	2.77	2.88	5.19	4.94				
0.4	2.77	2.90	5.17	4.96				
0.6	2.76	2.89	5.15	4.93	2.80	2.75	6.62	3.16
0.8	2.76	2.88	5.24	4.85	2.82	2.77	6.77	2.82
1.0	2.76	2.90	5.19	4.89	2.81	2.75	6.71	2.95

[a] Subindexes w and c refer to water and clay, respectively. Peak positions are given in Å.

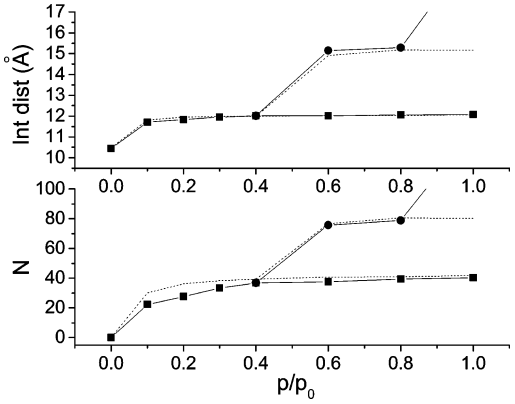

Figure 11. Interlaminar distance and number of water molecules per interlaminar space as a function of the vapor pressure for burial conditions. For comparison, the dotted line corresponds to ground conditions (from Figure 10).

Table 2 shows the main peak positions and the first shell coordination numbers for the systems equilibrated at different relative vapor pressures and for a single and a double water layer configurations. This was done to prove that the shifts of the water and clay peaks mentioned in the preceding section are indeed significant over a wide range of vapor pressures. As can be seen for the single layer hydrate, the K−O water clay position is practically constant and equal to the one found from the $NP_{zz}T$ sampling. Also the double layer p_w is close to the value found in the previous section, i.e, similar to the K−O bulk water position. On the other hand, p_c increases for increasing the relative water pressure, reaching a plateau at $p/p_0 \geq 0.3$. The plateau value is close to 2.89 Å, which is also similar to the value found in the preceding section. The decrease of this distance with p/p_0 is a consequence of the decrease of the interlaminar distance with it. For the double layer configuration it also confirmed a value close to 2.76 Å. Hence, the shifts of these peaks are relevant and not just casual values obtained for some particular conditions. From Table 2 it is seen that the values for the coordination numbers also agree with those presented in the previous section.

To evaluate the effect of the burial depth on the K-montmorillonite swelling curves, Figure 11 was built for $T = 394$ K and $P = 600$ atm. Additionally, results for ground level conditions were included to make the comparison easy. As can be seen, for initial conditions of 10 water molecules and a small interlaminar space, the interlaminar distance is slightly smaller than those obtained for ground level conditions. This combines with the fact that water molecules occupy a larger effective volume for burial conditions, and so, the number of water molecules decreases. In other words, the single layer hydrate of K-montmorillonite dehydrates under burial conditions. Furthermore, this single layer hydrate is stable even for a saturated water vapor pressure. Again, this contrasts with the results we obtained for Na-montmorillonite,[21] where the single layer hydrate was found to be unstable for large water activities. Moreover, for $p/p_0 = 1.0$, the K-montmorillonite single layer hydrate yields 12.07 Å of interlaminar space and 40.4 water molecules, which seems to be far from the transition range of 45−55 water molecules previously found.

The double layer hydrate behaves differently. That is, it keeps constant its water content, and it slightly increases its interlaminar distance. As found for ground level conditions, it collapses forming the single layer hydrate for $p/p_0 < 0.6$. On the other hand, for a saturated vapor pressure the system monotonically increases its amount of water as the simulation evolves. In this last case we stopped the simulations when reaching 180 water molecules, and thus, we assumed that the system entered the osmotic regime.

In summary, these results indicate that once formed the K-montmorillonite single water hydrate will not be destabilized neither at ground level conditions nor at burial depths. In addition, if the reservoir vapor pressure fells down $0.4p_0$ the single water hydrate will form.

IV. Discussion and Conclusions

Single and double layer hydrates of K-montmorillonite were studied by means of $NP_{zz}T$ and $\mu P_{zz}T$ simulations. For that purpose a hybrid Monte Carlo scheme was employed. Most results from the $NP_{zz}T$ sampling just confirm those previously reported elsewhere,[14,15,17−19] suggesting that differences in models and methods are not very important.

We found different clay−water−ion complexes for the single water hydrate. They consist of an average of 5 water molecules surrounding a potassium ion that additionally coordinates with two oxygen atoms of each closest clay layer. These potassium ions are placed at the interlayer midplane, and so, distances between them and the oxygens of the clay are slightly larger than those observed for the double layer hydrate. It should be mentioned that these midplane ions were reported by previous works as forming outer-sphere complexes.[14,16] In fact, Chang et al.[16] found that these midplane ions have a relatively large mobility, since potassium ions neither strongly coordinate to water molecules nor strongly interact with the clay surfaces. This is, indeed, characteristic of an outer-sphere complex. This explains why they call them in this way. Nonetheless, the inner-sphere definition given elsewhere[15] says literally "The surface complex is inner-sphere if the cation is bound directly to a cluster of surface oxygen ions, with no water molecules interposed". Accordingly, our midplane potassium ions form inner-sphere complexes but simultaneously with both clay layers. Nevertheless, we expect them to have a diffusivity similar to that reported by Chang et al.[15] This is a clear difference

between this kind of inner-sphere complex and the typical inner-sphere complex, where ions are strongly coordinated to one of the surfaces.[15] This simultaneous coordination of potassium ions with oxygen atoms of the two adjacent clay layers plus their relatively large coordination distances suggests to us that these complexes are attracting the clay layers toward the interlayer midplane, aiding to keep them together.

Although the previous finding seems to explain the stability of the single layer hydrate found experimentally, we should also reproduce computationally this behavior. Hence, $\mu P_{zz}T$ simulations were carried out. This ensemble lets interchange water with a given reservoir and volume fluctuations. So, for any given water vapor pressure of the reservoir, an average amount of water and an average interlaminar distance are found. However, two different equilibrium states may be produced, pointing to the formation of free energy local minima,[20] which are accessed by handling initial conditions. This produces hysteresis loops.[20] We found that for initial conditions close to the dehydrated state, a single water layer is always obtained for any nonzero vapor pressure, signaturing its high stability. The amount of water of this single layer slightly increases as the vapor pressure increases. This was obtained for ground level and burial conditions. The interlaminar distance for the ground level state is always close to 12.0 Å. The number of water molecules was found to be close to 38 for ground level conditions and about 36 for burial conditions. This is due to the larger effective volume the water molecules occupy at higher temperatures.

On the other hand, the stability of the double layer hydrate differs from that one of the single layer. For both conditions studied, it was seen that the double layer collapses to form the single layer for vapor pressures under $0.4p_0$. In addition, this double layer was found to be unstable for burial depth and for saturated vapor pressures, producing a hydrated state in the osmotic regime.

We should point out that these results agree with those of Boek et al.[14] In their Figure 3 is shown the potential energy of the interlayer water as a function of the number of water molecules. It can be seen that the potassium curve is very different than the sodium and lithium ones only for small amounts of water (it shows much higher energy values, even well above the water bulk reference). This supports our finding of an extremely stable single water hydrate. Nevertheless, they claim that potassium is a good swelling inhibitor due to its ability to migrate and bind to the clay surfaces. Hence, the negatively charged surface becomes screened, making its inherent repulsion less effective. We agree that this mechanism explains the relatively high stability of double layer hydrates and even explains the stability of K-montmorillonite hydrates in the osmotic regime. However, it cannot explain the remarkable stability of the single layer hydrate, since at least a double layer is needed to obtain the binding between ions and surfaces. This fact makes us think that midplane potassium ions are playing an important role in the stability of single layer hydrates.

Despite the thinking that the potassium simultaneously binding to adjacent layers is the key to the single layer hydrate stability, we do not think it is the only factor. Lowest interaction energy for the pair K-TIP4P water is close to −20 kcal, which is higher than that for Na-TIP4P of approximately −25 kcal. This means that potassium ion does not strongly interact with water, and, therefore, it easily loses water from its coordination shell. In other words, the water chemical potential of the interlayer is not very negative. That is, water may be more comfortable in bulk than in the interlayer, surrounding the ions. As mentioned by Sposito et al.,[19] potassium ions show a kind of "hydrophobic character", in the sense that they tend to interact with water molecules not only through their positive charge but also through solvent cage formation. Consequently, some of the water oxygen atoms may be easily exchanged by oxygen atoms from the clay surface.

Finally, for drilling purposes and based on our results, it seems to not be enough to add potassium to the mud in order to guarantee the single layer water formation and, in this way, avoid swelling. One should simultaneously decrease the mud water activity to safely produce the single layer state. Once obtained, the clay will not swell at all.

Acknowledgment. This research was supported by Instituto Mexicano del Petróleo Grant D.00072.

References

(1) Boek, E. S.; Conveney, P. V.; Skipper, N. T. *Langmuir* **1995**, *11*, 4629−4631.

(2) Boek, E. S.; Sprik, M. *J. Phys. Chem. B* **2003**, *107*, 3251−3256.

(3) Chávez-Páez, M.; de Pablo, L.; de Pablo, J. J. *J. Chem. Phys.* **2001**, *114*, 10948−10953.

(4) Chávez-Páez, M.; Van Workum, K.; de Pablo, L.; de Pablo, J. J. *J. Chem. Phys.* **2001**, *114*, 1405−1413.

(5) Chou Chang, F.; Skipper, N. T.; Sposito, G. *Langmuir* **1995**, *11*, 2734−2741.

(6) Chou Chang, F.; Skipper, N. T.; Sposito, G. *Langmuir* **1997**, *13*, 2074−2082.

(7) Hensen, E. J. M.; Smit, B. *J. Phys. Chem. B* **2002**, *106*, 12664−12667.

(8) Marry, V.; Turq, P. *J. Phys. Chem. B* **2002**, *107*, 1832−1839.

(9) Odriozola, G.; Guevara, F. *Langmuir* **2004**, *20*, 2010−2016.

(10) Smith, D. E.; Wang, Y.; Whitley, H. D. *Fluid Phase Equilib.* **2004**, *222−223*, 189−194.

(11) Sutton, R.; Sposito, G. *J. Colloid Interface Sci.* **2001**, *237*, 174−184.

(12) Whitley, H. D.; Smith, D. E. *J. Chem. Phys.* **2004**, *120*, 5387−5395.

(13) Young, D. A.; Smith, D. E. *J. Phys. Chem. B* **2000**, *104*, 9163−9170.

(14) Boek, E. S.; Coveney, P. V.; Skipper, N. T. *J. Am. Chem. Soc*. **1995**, *117*, 12608−12617.

(15) Chang, F.; Skipper, N. T.; Refson, K.; Greathouse, J.; Sposito, G. In *ACS Symposium Series No. 715*; Schultz, L., van Olphen, H., Mumpton, F., Eds.; American Chemical Society: Washington, DC, 1999.

(16) Chou Chang, F.; Skipper, N. T.; Sposito, G. *Langmuir* **1998**, *14*, 1201−1207.

(17) Hensen, E. J. M.; Tambach, T. J.; Bliek, A.; Smit, B. *J. Chem. Phys*. **2001**, *115*, 3322−3329.

(18) Park, S.; Sposito, G. *J. Phys. Chem. B* **2000**, *104*, 4642−4648.

(19) Sposito, G.; Skipper, N. T.; Sutton, R.; Park, S. H.; Soper, A. K.; Greathouse, J. *Proc. Natl. Acad. Sci.* **1999**, *96*, 3358−3364.

(20) Tambach, T. J.; Hensen, E. J. M.; Smit, B. *J. Phys. Chem. B* **2004**, *108*, 7586−7596.

(21) Odriozola, G.; Aguilar, F.; López-Lemus, J. *J. Chem. Phys.* **2004**, *121*, 4266−4275.

(22) Tambach, T. J.; Bolhuis, P. G.; Smit, B. *Angew. Chem., Int. Ed.* **2004**, *43*, 2650−2652.

(23) Skipper, N. T.; Chou Chang, F.; Sposito, G. *Clays Clay Miner.* **1995**, *43*, 285−293.

(24) Jorgensen, W. L.; Chandrasekhar, J.; Madura, J. D. *J. Chem. Phys*. **1983**, *79*, 926−935.

(25) Marry, V.; Turq, P.; Cartailler, T.; Levesque, D. *J. Chem. Phys*. **2002**, *117*, 3454−3463.

(26) Bounds, D. G. *Mol. Phys*. **1985**, *54*, 1335−1355.

(27) Tongraar, A.; Liedl, K. R.; Rode, B. M. *J. Phys. Chem. A* **1998**, *102*, 10340−10347.

(28) Neilson, G. W.; Skipper, N. T. *Chem. Phys. Lett*. **1985**, *114*, 35−38.

(29) Ohtaki, H.; Radnai, T. *Chem. Rev.* **1993**, *93*, 1157−1204.

(30) Mehlig, B.; Heermann, D. W.; Forrest, B. M. *Phys. Rev. B* **1992**, *45*, 679−685.

(31) Alejandre, J.; Tildesley, D. J.; Chapela, G. A. *J. Chem. Phys.* **1994**, *102*, 4574−4583.

(32) Allen, M. P.; Tildesley, D. J. *Computer Simulation of Liquids;* Clarendon: Oxford, 1986.

(33) Tuckerman, M.; Berne, B. J. *J. Chem. Phys.* **1992**, *97*, 1990−2001.

(34) Frenkel, D.; Smit, B. *Understanding molecular simulation;* Academic: New York, 1996.

(35) Different types of movements should be called randomly, otherwise detail balance is violated.[34] The data published here and in refs 9 and 21 were obtained by following this sequential algorithm. However, some data were checked by means of the corresponding random algorithm, and the same results were obtained.

(36) Calvet, R. *Ann. Agron*. **1973**, *24*, 77−133.

(37) de Pablo, L.; Chávez, M. L.; Sum, A. K.; de Pablo, J. J. *J. Chem. Phys*. **2004**, *120*, 939−946.

(38) Skipper, N. T.; Williams, G. D.; de Siqueira, A. V. C.; Lobban, C.; Soper, A. K. *Clay Miner*. **2000**, *35*, 283−290.

(39) Bérend, I.; Cases, J. M.; François, M.; Uriot, J. P.; Michot, L.; Masion, A.; Thomas, F. *Clays Clay Miner*. **1995**, *43*, 324−336.

(40) Sato, T.; Watanabe, T.; Otsuka, R. *Ann. Agron*. **1992**, *40*, 103−113.

(41) Brindley, G. W.; Brown, G. *Crystal Structures of Clay Minerals and their X-ray Identification*, 5th ed.; Mineralogical Society: London, 1984.

CT050062L